

# Comparative study of cost-effective coherent and direct detection schemes for 100 Gb/s/ $\lambda$ PON

YIXIAO ZHU,<sup>1</sup> LILIN YI,<sup>1</sup> BO YANG,<sup>2</sup> XINGANG HUANG,<sup>2</sup> JUN SHAN WEY,<sup>3</sup> ZHUANG MA,<sup>2</sup> AND WEISHENG HU<sup>1,\*</sup> 

<sup>1</sup>State Key Laboratory of Advanced Optical Communication Systems and Networks, Department of Electronic Engineering, Shanghai Jiao Tong University, Shanghai 200420, China

<sup>2</sup>ZTE Corporation, Shanghai 201203, China

<sup>3</sup>ZTE Tx Inc., Morristown, New Jersey 07960, USA

\*Corresponding author: wshu@sjtu.edu.cn

Received 18 February 2020; revised 11 May 2020; accepted 12 May 2020; published 3 June 2020 (Doc. ID 390911)

As the capacity of the next-generation passive optical network (PON) is reaching 100 Gb/s and beyond, cost-effective transceivers have been widely discussed. In this work, we provide a comprehensive comparison of various simplified coherent and direct detection (DD) schemes operating at a 100 Gb/s/ $\lambda$  4-ary pulse amplitude modulation signal through numerical simulation. According to the cost, the coherent receivers can be divided into three levels: intensity-only coherent receivers and phase-insensitive and phase-sensitive complex-value coherent receivers. The received power sensitivity at back-to-back, influence of laser frequency offset, local oscillator power, laser linewidth, analog-to-digital convertor resolution, fiber dispersion, and hardware complexity are investigated and analyzed for each transceiver structure. The results show the following: (1) Transmitter-side optical amplification is suggested for DD and intensity-only coherent receivers to meet the 29 dB power budget requirement, and these schemes have a large dispersion penalty. (2) Compared with 3  $\times$  3 coupler and 2  $\times$  4 hybrid-based coherent receivers, 2  $\times$  2 coupler and balanced-photodiode-based heterodyne detection exhibit similar performance with a simpler structure. (3) Both phase-insensitive and phase-sensitive complex-value coherent receivers have superior power budget and dispersion tolerance, and their application in PON would depend on the cost. © 2020 Optical Society of America

<https://doi.org/10.1364/JOCN.390911>

Provided under the terms of the OSA Open Access Publishing Agreement

## 1. INTRODUCTION

The advent of the 5G Era, 4K/8K high-definition video, cloud computing, the Internet of Things (IoT), and other broadband services have put forward higher bandwidth requirements for access networks. A passive optical network (PON), which utilizes a point-to-multipoint tree topology architecture based on a power splitter, can provide a cost-effective access solution. In December 2015, the IEEE 802.3ca Task Force started to standardize for next-generation 25G/50G/100G PON [1]. Originally, 100 Gb/s was proposed by multiplexing four wavelengths each at the bit rate of 25 Gb/s, and later on the target was reduced to 50 Gb/s considering the technological maturity and the market demand, where two 25 Gb/s channels are bonded [2,3]. In 2018, the ITU Telecommunication Standardization Sector (ITU-T) Question 2/Study Group 15 (Q2/SG15) launched the process to standardize a single wavelength 50G-PON [4]. Recently, there is growing attention on 100 Gb/s/ $\lambda$  PON research [5–8]. For example, Ref. [5] reports the first experimental demonstration of 100 Gb/s/ $\lambda$

4-ary pulse amplitude modulation (PAM-4) O-band transmission with direct detection (DD), in which a 29 dB power budget is achieved with a 10G-class directly modulated laser (DML) and receiver-side semiconductor optical amplifier (SOA) pre-amplification. Assisted by an artificial neural network (ANN)-based equalization, a 100 Gb/s PAM-8 signal is also feasible by using a 20G-class device and both pre- and post-amplification [6]. Although intensity modulation (IM)-DD links are still possible to support future single-wavelength 100G-PON, the loss budget is quite challenging and the fiber dispersion would become a more severe impairment.

Apart from direct detection, coherent detection has also been considered as a promising candidate. First, a local oscillator (LO) laser at the receiver would beat with the signal during photodiode (PD) detection, leading to improved receiver sensitivity. Second, different from the square-law detection of IM-DD links, the coherent receivers can recover the linear optical field with both amplitude and phase information. Therefore, the fiber dispersion induced power fading effect [9] can be avoided and the inter-symbol interference (ISI)

would be efficiently mitigated with an equalizer. Moreover, the coherent receiver can detect the channel of interest by tuning the wavelength of the LO without an optical filter, making the network more flexible, especially in the wavelength division multiplexing (WDM) case. However, the cost of a typical coherent transceiver is still too high for the cost sensitive access market.

To address the cost issue, a number of simplified coherent detection architectures are proposed [7,8,10–13]. In Ref. [10], 25 Gb/s upstream is experimentally demonstrated with non-return-to-zero (NRZ) modulation and a simple  $3 \times 3$  fiber splitter-based coherent detection. By using phase-insensitive heterodyne coherent detection, a 100 Gb/s PAM-4 signal transmission with a 32 dB loss budget is realized [7]. Furthermore, with the help of phase recovery, a maximum power budget of 32.5 dB has been reported for a 200 Gb/s/ $\lambda$  polarization division multiplexed (PDM) PAM-4 signal over 20 km fiber transmission at the C-band [8]. Note that since a manual polarization controller is used in Ref. [7], an additional 3 dB sensitivity penalty is expected if a polarization-diversity coherent receiver is employed for practical implementation. Alternatively, polarization-independent coherent detection can be realized by adopting Alamouti coding [11–13]. Reference [12] reports a 50 Gbaud quadrature phase shift keying (QPSK) signal-based 100 Gb/s PON by employing a dual-polarization IQ modulator and  $2 \times 2$  coupler-based heterodyne detection. The loss budget is 36.6 dB after 80 km standard single-mode fiber (SSMF) transmission at the C-band. As a modification, real-valued Alamouti-coded 56 Gb/s/ $\lambda$  PAM-4 is also demonstrated, offering 41 dB after 50 km SSMF transmission [13].

Since there are various simplified coherent detection architectures, an important task would be to compare the performance of these schemes. Previously, Ref. [14] reviewed the principle of quasi-coherent and polarization-independent coherent receivers, split carrier transmitters, hybrid transmitter-receiver externally modulated lasers (EMLs), and Kramers–Kronig (KK) detection. Reference [15] compares the sensitivity of five receiver structures with a 10 Gb/s on-off keying (OOK) signal in terms of the number of photons per bit (PPB). Reference [16] introduces the structure of bidirectional intradyne, heterodyne, and self-homodyne coherent PON. However, most of the aforementioned work focuses on comparing received power sensitivity at back-to-back (BTB), and other performance metrics such as laser frequency offset, laser phase noise, and dispersion tolerance are not fully analyzed [14–16].

In this work, we provide a comprehensive comparison of 15 cost-effective coherent detection and DD schemes operating with a 100 Gb/s/ $\lambda$  PAM-4 signal through numerical simulation. As an extension of our previous work [17], we upgrade the target from 50G-PON to future 100 Gb/s/ $\lambda$  PON, and provide more detailed analysis. Different from Ref. [17], we investigate three levels of coherent receivers according to the cost: (1) with analog process circuit-based intensity-only reception, (2) with phase-insensitive complex-value reception, and (3) with phase-sensitive complex-value reception. Furthermore, to meet the requirement of practical implementation, the receiver sensitivity at BTB, the influence of laser

frequency offset, LO power, laser linewidth, analog-to-digital convertor (ADC) resolution, fiber dispersion, and hardware complexity are also quantitatively studied.

The remainder of the paper is organized as follows. In Section 2, simplified coherent detection and DD transceiver structures as well as the DSP stack are introduced. Section 3 presents the simulation results and provides corresponding explanations in terms of different system parameters. Finally, conclusions are drawn in Section 4.

## 2. TRANSCEIVER STRUCTURE AND DSP STACK

In this section, the transceiver architectures are classified into 4 categories: 1) DD receiver, 2) analog process circuit-based intensity-only coherent receiver, 3) phase-insensitive complex-value coherent receiver, and 4) phase-sensitive complex-value coherent receiver.

### A. DD Receiver

For DD schemes, EML + SOA + PIN and EML + APD are considered, as in Figs. 1(a), 1(d), and 1(e). At the transmitter, although the cost of a DML is lower than an EML, a DML model consisting of transient and adiabatic chirp is more complicated. Therefore, the EML in Fig. 1(a) is employed here. In the EML model, a continuous-wave (CW) laser is used as an optical source, and an electro-absorption modulator (EAM) performs intensity modulation. At the receiver, an avalanche photodiode (APD) and the combination of a SOA and a positive-intrinsic-negative (PIN) PD are tested; see Figs. 1(d) and 1(e), respectively. Benefiting from the avalanche gain, an APD is an economic solution to meet the requirement of loss budget for an existing PON. As the bit rate gets higher, SOA + PIN becomes competitive to enhance the receiver sensitivity with the help of optical amplification. In this paper, DD receivers are used as a benchmark for a performance comparison of different coherent detection schemes.

### B. Intensity-Only Coherent Receiver

For simplified intensity-only coherent detection schemes, a  $2 \times 2/3 \times 3$  coupler-based heterodyne, a  $3 \times 3$  coupler, and a  $2 \times 4$  hybrid-based intradyne receiver are compared in Figs. 1(f)–1(k). An EML is still used at the transmitter for single-polarization intensity modulation to reduce the cost. Figure 1(f) shows the  $2 \times 2$  coupler and single-ended PD (SPD)-based heterodyne detection scheme ( $2 \times 2$  SPD Het. Rx) [18]. The receiver consists of two parts: an O/E front-end and an analog process circuit. Note that the practical  $2 \times 1$  coupler is realized by leaving one output of the  $2 \times 2$  coupler unused. Assuming the optical field of the received signal and the LO to be  $[E_x, E_y]^T$  and  $[L, L]^T$ , then the output photocurrent of each polarization can be obtained as follows:

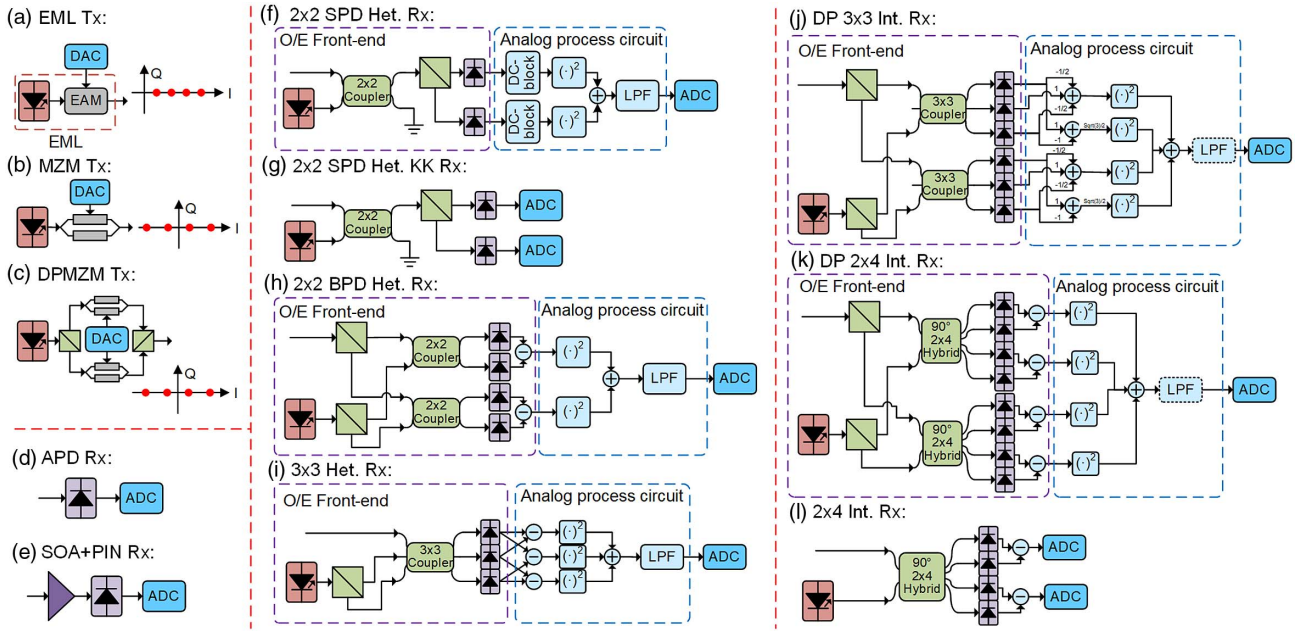


**Fig. 1.** Transmitter and receiver structures of DD and coherent detection schemes. Tx, transmitter; Rx, receiver; DAC, digital-to-analog converter; ADC, analog-to-digital converter; EML, external modulated laser; EAM, electro-absorption modulator; MZM, Mach-Zehnder modulator; DP, dual-polarization; SOA, semiconductor optical amplifier; PIN, positive-intrinsic-negative; SPD, single-ended photodiode; BPD, balanced photodiode; LPF, low-pass filter; Het., heterodyne; Int., intradyne.

$$\begin{aligned}
 I_{x/y} &\propto \left| \frac{L + E_{x/y}}{\sqrt{2}} \right|^2 = \frac{|L|^2 + 2\text{Re}\{E_{x/y} \cdot L^*\} + |E_{x/y}|^2}{2} \\
 &\approx \frac{|L|^2 + 2\text{Re}\{E_{x/y} \cdot L^*\}}{2} \\
 &= \frac{2|E_{x/y}||L| \cos(\Delta\omega t + \Delta\varphi) + |L|^2}{2}. \quad (1)
 \end{aligned}$$

Here  $(\cdot)^T$  denotes the transpose operation,  $\Delta\omega$  is the frequency offset between the transmitter-side EML and the LO, and  $\Delta\varphi$  is the phase noise. The signal-signal beating interference (SSBI) is neglected since the power of the LO is much larger than the signal in the PON scenario. In the analog process circuit, the LO-LO beating term is first removed by a direct-current (DC) block. After a square and add operation, the waveform is

$$\begin{aligned}
 r &= I_x^2 + I_y^2 = \frac{1 + \cos(2\Delta\omega t + 2\Delta\varphi)}{2} \\
 \cdot (|E_x|^2 + |E_y|^2)|L|^2 &= \frac{1 + \cos(2\Delta\omega t + 2\Delta\varphi)}{2} |L|^2 S. \quad (2)
 \end{aligned}$$

The first and second terms are located at the frequency of 0 and  $2\Delta\omega$ , respectively. After the low-pass filter (LPF), most of the second-order term can be removed, and thus the output is proportional to the signal thanks to intensity modulation.

Recently, KK detection has been widely used in a single sideband (SSB) DD system [19–21] and a heterodyne coherent detection system [22,23]. Figure 1(g) shows the structure of the  $2 \times 2$  coupler-based heterodyne KK detection scheme ( $2 \times 2$  SPD Het. KK Rx). The O/E front-end is the same as the  $2 \times 2$  SPD Het. Rx, while in the receiver-side DSP, the complex optical field  $E'_{x/y}$  can be reconstructed without SSBI

as follows:

$$\begin{aligned}
 \phi_{x/y}(t) &= H \left[ \ln(\sqrt{I_{x/y}}) \right], \\
 E'_{x/y} &= \sqrt{I_{x/y}} \exp[j\phi_{x/y}(t)]. \quad (3)
 \end{aligned}$$

Here  $H[\cdot]$  represents the Hilbert transform. For simplified intensity-only reception, the outputs are then squared with the modulus value and added to recover the transmitted signal.

Figure 1(h) depicts the  $2 \times 2$  coupler and balanced PD (BPD)-based heterodyne detection ( $2 \times 2$  BPD Het. Rx) [8]. In this architecture, the output photocurrent of each BPD is given as follows:

$$\begin{aligned}
 I_{x/y} &\propto \left| \frac{L + E_{x/y}}{\sqrt{2}} \right|^2 - \left| \frac{L - E_{x/y}}{\sqrt{2}} \right|^2 = 2\text{Re}\{E_{x/y} \cdot L^*\} \\
 &= 2|E_{x/y}||L| \cos(\Delta\omega t + \Delta\varphi). \quad (4)
 \end{aligned}$$

We can find that the SSBI terms are canceled, and the signal-LO beating term is doubled compared with SPD detection. The process in the following analog circuit is similar to that in Eq. (2).

In addition to a  $2 \times 2$  coupler, a  $3 \times 3$  coupler can also be used for heterodyne detection ( $3 \times 3$  Het. Rx) as in Fig. 1(i) [10,24]. The signal and LO are mixed as follows [25]:

$$\begin{aligned}
 \begin{pmatrix} a & b & b \\ b & a & b \\ b & b & a \end{pmatrix} \begin{pmatrix} E_x & E_y \\ 0 & L \\ L & 0 \end{pmatrix} &= \begin{pmatrix} aE_x + bL & aE_y + bL \\ bE_x + bL & bE_y + aL \\ bE_x + aL & bE_y + bL \end{pmatrix}, \\
 a &= 2 \exp(j2\pi/9)/3 + \exp(-j4\pi/9)/3, \\
 b &= \exp(-j4\pi/9)/3 - \exp(j2\pi/9)/3. \quad (5)
 \end{aligned}$$

After PD detection, the photocurrents are subtracted from each other to mitigate the second-order beating terms. Therefore, with a square and add operation, the output is calculated as follows [26]:

$$r = (I_1 - I_2)^2 + (I_2 - I_3)^2 + (I_3 - I_1)^2 \\ \propto \frac{2}{3} \left( 1 - \sin(2\theta) \sin \left( \frac{\pi}{6} - 2\Delta\omega t - \Delta\varphi \right) \right) |L|^2 S. \quad (6)$$

Here  $\theta$  is the azimuthal angle of signal polarization. Although the second term is polarization dependent, it can be suppressed by the following LPF.

In addition to the heterodyne receiver, the intradyne receiver is another category of a coherent receiver structure. Here homodyne detection is included as a particular case of intradyne detection, where the frequency of the LO coincides with the signal. For a  $3 \times 3$  coupler-based polarization-diversity intradyne receiver ( $3 \times 3$  DP Int. Rx), as shown in Fig. 1(j) [27], both the signal and LO need to be divided by a polarization beam splitter (PBS) before entering optical couplers. In this case, the photocurrents of each PD are given as follows:

$$I_{x1/y1} \propto |aE_{x/y} + bL|^2 \\ \approx \left[ |E_{x/y}|^2 + 2|E_{x/y}||L| \cos \left( \Delta\varphi + \frac{2}{3}\pi \right) + |L|^2 \right] / 3, \\ I_{x2/y2} \propto |bE_{x/y} + bL|^2 \\ \approx \left[ |E_{x/y}|^2 + 2|E_{x/y}||L| \cos(\Delta\varphi) + |L|^2 \right] / 3, \\ I_{x3/y3} \propto |bE_{x/y} + aL|^2 \\ \approx \left[ |E_{x/y}|^2 + 2|E_{x/y}||L| \cos \left( \Delta\varphi - \frac{2}{3}\pi \right) + |L|^2 \right] / 3. \quad (7)$$

In the analog process stage, linear combination recovers the in-phase/quadrature components of each polarization, and the transmitted signal is finally obtained as in Eq. (8). Note that the LPF is not necessary for intradyne receivers; we just keep it for fair comparison:

$$r_{xI/yI} = I_{x2/y2} - 0.5(I_{x1/y1} + I_{x3/y3}) = |E_{x/y}||L| \cos \Delta\varphi, \\ r_{xQ/yQ} = \frac{\sqrt{3}}{2}(I_{x1/y1} - I_{x3/y3}) = |E_{x/y}||L| \sin \Delta\varphi, \\ r = r_{xI}^2 + r_{xQ}^2 + r_{yI}^2 + r_{yQ}^2 = |L|^2 S. \quad (8)$$

Figure 1(k) shows the  $2 \times 4$  DP  $90^\circ$  hybrid-based intradyne detection receiver ( $2 \times 4$  DP Int. Rx). After the PBS and optical hybrid, the output photocurrents in Eq. (9) equal the I/Q components of two polarizations, respectively. Then the signal can be acquired by squaring and adding.

$$I_{xI/yI} \propto \left| \frac{E_{x/y} + L}{2} \right|^2 - \left| \frac{E_{x/y} - L}{2} \right|^2 = \text{Re}\{E_{x/y} \cdot L^*\}, \\ I_{xQ/yQ} \propto \left| \frac{E_{x/y} + jL}{2} \right|^2 - \left| \frac{E_{x/y} - jL}{2} \right|^2 = \text{Im}\{E_{x/y} \cdot L^*\}, \\ r = r_{xI}^2 + r_{xQ}^2 + r_{yI}^2 + r_{yQ}^2 = |L|^2 S. \quad (9)$$

### C. Phase-Insensitive Complex-Value Coherent Receiver

Different from intensity-only coherent receivers, phase-insensitive complex reception needs to get both the amplitude and phase information to recover the optical field. Therefore, the  $2 \times 2$  SPD Het. Rx,  $2 \times 2$  SPD Het. KK Rx,  $2 \times 2$  BPD Het. Rx,  $3 \times 3$  Het. Rx,  $3 \times 3$  DP Int. Rx, and  $2 \times 4$  DP Int. Rx in Figs. 1(f)–1(k) can be easily modified, by keeping the O/E front-end and removing the analog process circuit.

On the other hand, phase-insensitive complex-value coherent receivers deal with the information of the linear optical field in the receiver-side DSP. Before being modulated onto the EML, a PAM-4 signal is added with a DC component according to the modulation index and then pre-distorted by using a square root operation. In doing so, the optical amplitude of the EML is equally spaced as in Ref. [7], rather than the optical power.

### D. Phase-Sensitive Complex-Value Coherent Receiver

In this subsection, the Mach–Zehnder modulator (MZM)-based transmitter in Figs. 1(b) and 1(c) and the  $2 \times 4$  hybrid-based intradyne receiver in Figs. 1(k) and 1(l) are introduced. To achieve further improvement, the combination of the MZM and the polarization-diversity intradyne receiver in Fig. 1(k) is a feasible scheme (MZM +  $2 \times 4$  DP Int. Rx). At the transmitter, the MZM is biased at the null point to suppress the optical carrier, and thus the receiver sensitivity can be increased. Besides, since the signal level is located at  $-3, -1, 1, 3$  in this scenario, phase recovery is needed before making a decision. This scheme is similar to the standard IQ modulation coherent detection systems, except for not using the quadrature dimension to encode information.

As mentioned in Section 1, the polarization diversity can be moved from the receiver to the transmitter by adopting Alamouti coding [11–13] to reduce the ONU complexity as in Fig. 1(l). The Alamouti coding can be understood as polarization-time block coding, which transmits adjacent symbols  $[s_1, s_2]^T$  in the two polarizations of the first symbol period, and their conjugated pairs  $[-s_2^*, s_1^*]^T$  at the second symbol period, respectively. In doing so, the signal polarization switches to its orthogonal state during the coding block. Therefore, it is possible for a single-polarization  $2 \times 4$  optical hybrid to detect the signal. Note that both  $2 \times 2$  coupler-based heterodyne detection and  $3 \times 3$  coupler-based intradyne detection are feasible at the receiver [11, 12]; we take the  $2 \times 4$  DP Int. Rx. as a representative scheme. In addition, for PAM-4

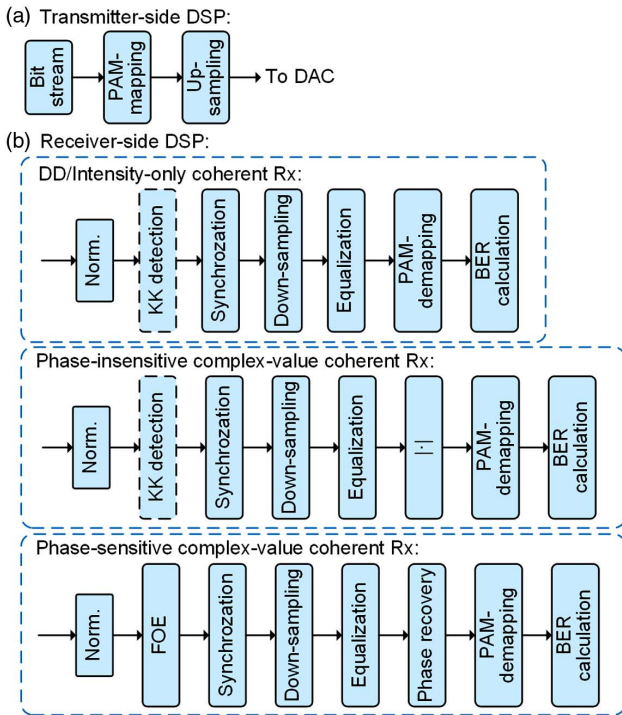


**Fig. 2.** (a) Transmitter-side and (b) receiver-side DSP stack. DD, direct detection; Rx, receiver; Norm., normalization; KK, Kramers–Kronig; FOE, frequency offset estimation.

signal transmission, Alamouti coding can be simplified to a real-valued version, and the DP-MZM in Fig. 1(c) is enough instead of a DP IQ modulator.

### E. DSP Stack

Figures 2(a) and 2(b) display the transmitter- and receiver-side DSP. At the transmitter, a binary bit stream is mapped into PAM-4 symbols. No pulse shaping or dispersion pre-compensation is performed. At the receiver, simplified intensity-only coherent receivers share the same DSP flow as DD receivers. First, the waveform is normalized to unit power. Afterwards, the signal is synchronized according to the cross correlation of the transmitted and received 64-symbol synchronization sequence. Before being sent to the equalizer, the signal is down-sampled to 2 samples per symbol (SPSs) considering both computational complexity and performance. In this work, linear channel equalization is performed in the time domain. The channel response is estimated based on the 1024-symbol training sequence, in which the filter taps are updated by using the recursive least square (RLS) algorithm for fast convergence. Then the equalizer is convoluted with the following data symbols. Finally, after decision, the bit error rate (BER) is calculated by error counting.

For phase-insensitive complex coherent receivers, the input I/Q waveforms are combined into complex values and normalized. In the training sequence-based time domain equalization, radial error is used to update taps. Multi-modulus algorithm (MMA)- or radius directed algorithm (RDA)-based blind equalization are also effective for ISI mitigation [28]. After equalization, there are four rings on the constellation, which

will be verified in Fig. 3. Finally, since no information is carried on the phase, a symbol decision can be made after modulus operation.

For phase-sensitive complex-value coherent receivers, the FOE algorithm needs to be modified because the MZM is biased at the null point. Fortunately, the differential phase-based method can be employed for the carrier-suppressed signal [29]. Afterwards, equalization is used to suppress the ISI. Before symbol decision, phase recovery is performed based on pilot symbols.

## 3. RESULTS AND DISCUSSION

The numerical simulation is carried out in VPITransmissionMaker. We investigate the performance of the aforementioned coherent detection and DD schemes with a 50 Gbaud PAM-4 signal for future 100 Gb/s/λ PON. To reduce the requirement of DAC resolution, no digital pulse shaping is used. For signal modulation, linear regions of an EML and MZM are utilized. The bandwidth of the EML/MZM and the APD/PD are set as 35 GHz with the 4th-order Bessel type in order to represent the 50G-class device. The relative intensity noise (RIN) is neglected for the model of the LO. Besides, it should be noted that an  $8\times$  up-sampling rate is used here; therefore, optical noise from the SOA is added within the 400 GHz optical simulation bandwidth for the SOA + PIN receiver. The rest of the simulation parameters are listed in Table 1.

Figure 3 displays the typical eye diagrams and constellations for simplified coherent detection and DD schemes at different received optical powers, respectively. We can find the following: (1) For intensity-only coherent receivers, the lower eye is more concentrated than the upper eye. The reason is that the PD noise is added with the signal, and the following square

**Table 1.** Simulation Parameters

Device	Parameter	Value
EML	Extinction ratio	7 dB
	Transient chirp factor	1
	Launch power	5 dBm
	Linewidth	10 MHz
MZM	Extinction ratio	100 dB
	Bias	Null point
APD	Avalanche multiplication factor	8
	Ionization coefficient	0.15
PD	Dark current	$600 \times 10^{-9}$ A
	Dark current	$3 \times 10^{-9}$ A
APD/PD	Responsivity	0.7 A/W
	Thermal noise	$10 \times 10^{-12}$ A/Hz <sup>1/2</sup>
SOA	Shot noise	On
	Gain	17 dB
LO	Noise figure	7 dB
	Linewidth	10 MHz
LPF	Power	15 dBm
	Bandwidth	25 GHz
$2 \times 2/3 \times 3/2 \times 4$ coupler/hybrid	Insertion loss	0 dB

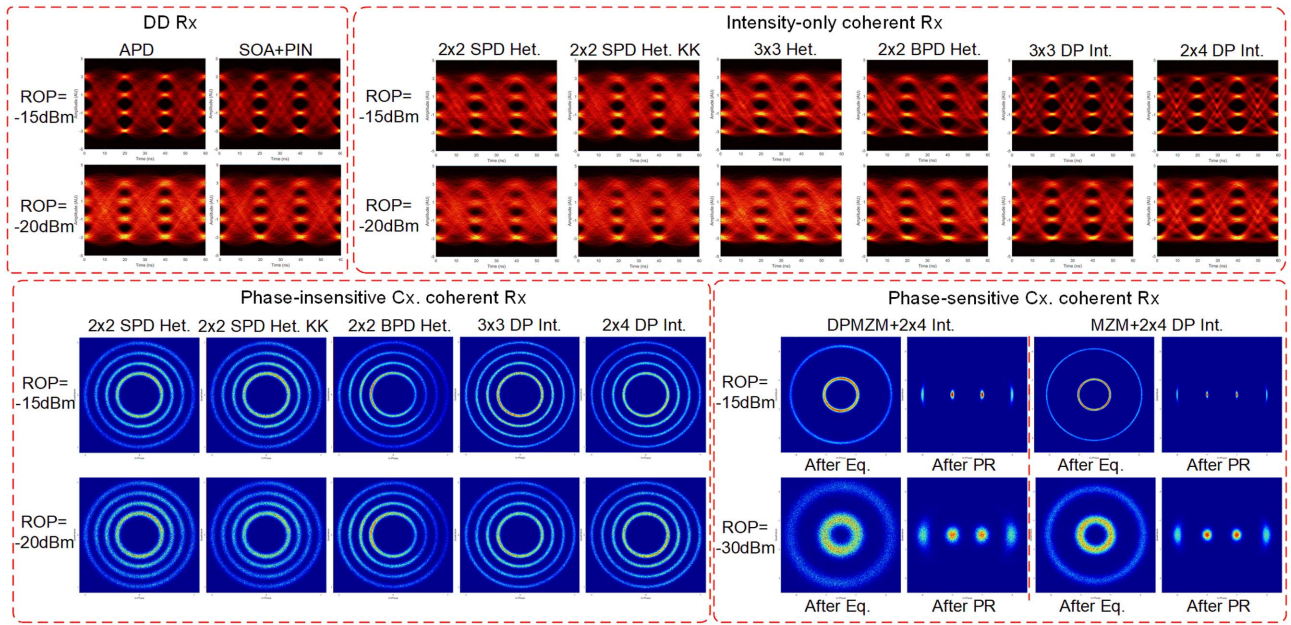


**Fig. 3.** Typical eye diagrams and constellations of simplified coherent detection and DD schemes at different received optical power, respectively. ROP, received optical power; Het., heterodyne; Int., intradyne; Cx., complex-value; Eq., equalization; PR, phase recovery.

operation generates the signal-noise beating term, which is pattern dependent. It should be noted that the SOA + PIN scheme has a similar phenomenon, where optical noise is induced by the SOA and then the signal-noise beating term is brought by PD detection. Therefore, better performance can be expected if an unequally spaced PAM-4 signal is used at the transmitter [30] or if a nonlinear equalizer (e.g., Volterra equalizer [31], artificial neural network [6,32]) is used at the receiver. (2) For phase-insensitive complex-value coherent receivers, the constellation can be successfully converged to four rings after equalization, while the symbols are rotated by the chirp of an EML and laser phase noise. (3) For phase-sensitive complex-value coherent receivers, the constellation converges to two rings after equalization, where  $\{-3, 3\}$  and  $\{-1, 1\}$  share the same modulus, respectively. Pilot symbol-based phase recovery is enough to separate four kinds of symbols, even with 10 MHz lasers.

To get a better understanding of the impact of the PD bandwidth, we plot the signal power spectral density (PSD) of  $2 \times 2$  BPD-based heterodyne and  $2 \times 4$  DP intradyne coherent receivers at  $-15$  dBm received optical power with phase-insensitive complex-value reception, respectively. The frequency offset between the LO and signal is set as 35 GHz and 0 GHz in Figs. 4(a) and 4(b), respectively. The S21 curve of the PD is also provided. Obviously, one of the signal sidebands is severely suppressed by the PD bandwidth after heterodyne detection, while the signal spectrum remains almost unchanged with homodyne/intradyne detection. Therefore, given the same receiver bandwidth, a larger penalty would be expected for the heterodyne receiver owing to the ISI.

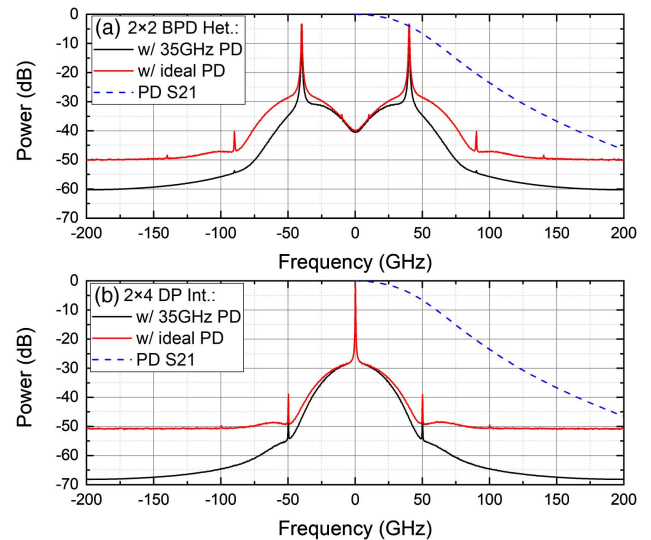


**Fig. 4.** Received power spectral density of (a)  $2 \times 2$  BPD-based heterodyne and (b)  $2 \times 4$  DP intradyne coherent receivers with phase-sensitive complex-value reception, respectively. w/, with.

### A. Receiver Sensitivity at BTB

Loss budget is a critical parameter for PON systems, which indicates the maximum number of ONUs that can be supported by a power splitter. Figure 5 displays the simulated receiver power sensitivity of DD and coherent receivers at BTB. In this simulation, the DAC and ADC have infinite resolution. The frequency offset between the transmitter-side laser and the LO are optimized as 40 GHz for heterodyne detection systems. At a BER threshold of  $1 \times 10^{-2}$ , the sensitivity of different schemes can be sorted from the least to the most sensitive as in Table 2. In order to simplify the text content in the

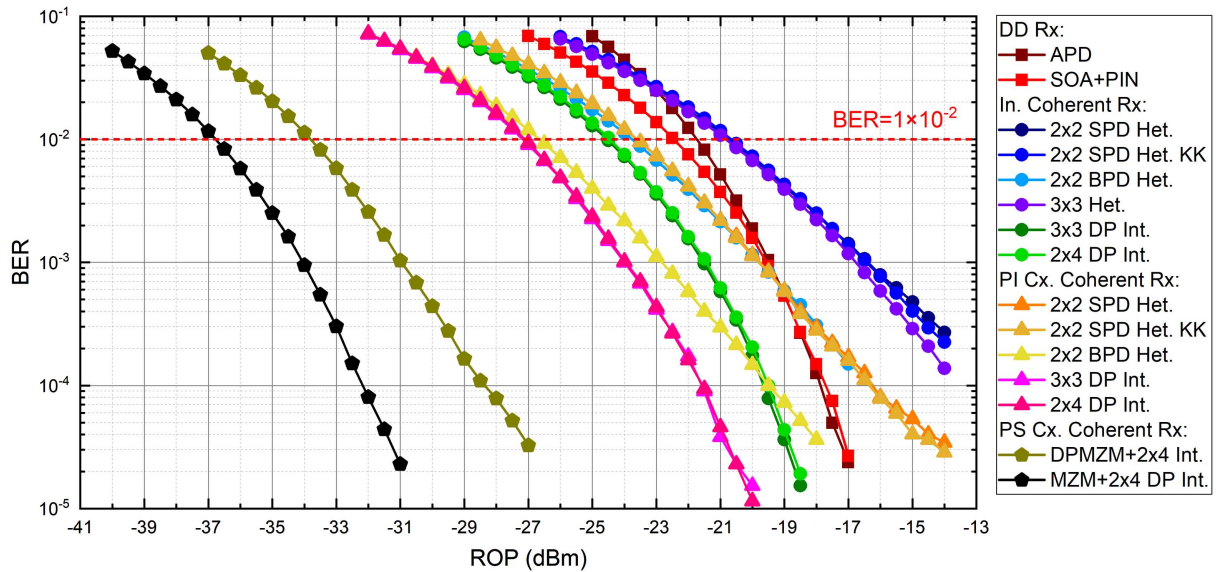


**Fig. 5.** Simulated receiver power sensitivity of DD, intensity-only, phase-insensitive, and phase-sensitive coherent detection schemes at back-to-back scenario. ROP, received optical power; In., intensity-only; PI, phase-insensitive; PS, phase-sensitive; Cx., complex-value.

**Table 2.** Receiver Sensitivity at  $BER = 1 \times 10^{-2}$

Category	Scheme	Sensitivity (dBm)
Intensity-only CRx	2 × 2 SPD Het.	−20.7
	2 × 2 SPD Het. KK	
	3 × 3 Het.	
DD Rx	APD	−21.7
DD Rx	SOA + PIN	−22.5
Intensity-only CRx	2 × 2 BPD Het.	−23.7
Phase-insensitive CRx	2 × 2 SPD Het.	−24.5
	2 × 2 SPD Het. KK	
	3 × 3 Het.	
Intensity-only CRx	3 × 3 DP Int.	−24.5
	2 × 4 DP Int.	
Phase-insensitive CRx	2 × 2 BPD Het.	−26.7
Phase-insensitive CRx	3 × 3 DP Int.	−27.1
	2 × 4 DP Int.	
Phase-sensitive CRx	DPMZM + 2 × 4 Int.	−33.8
Phase-sensitive CRx	MZM + 2 × 4 DP Int.	−36.8

table, the EML transmitter is neglected for DD and intensity-only and phase-insensitive complex-value coherent receivers. Besides, MZMs/DPMZMs are mentioned because they are specialized for the phase-sensitive complex-value coherent receiver only.

Based on the simulation results, we can get a better understanding about the above schemes. First of all, KK detection shows no advantage compared with SPD heterodyne detection. This is because the LO-to-signal power ratio is sufficiently large at the BER threshold, and SSBI is thus an insignificant impairment. Second, BPD heterodyne exhibits 3 dB sensitivity improvement compared with SPD heterodyne detection. It can be explained as one of the 2 × 2 coupler outputs is unused for SPD-based detection, so that half of the signal power is wasted. Similarly, the 2 × 2 coupler-based BPD heterodyne receiver has almost the same sensitivity as the 3 × 3 coupler/2 × 4

hybrid-based intradyne receiver. Ideally, heterodyne receivers require PDs with a higher bandwidth to detect I/Q components together at the intermediate frequency (IF). Given the same PD bandwidth in this simulation, the heterodyne receiver is thus slightly worse than intradyne receivers, due to the ISI. Such a penalty can be reduced if the PD bandwidth is larger than 50 GHz. Third, the same O/E front-end, phase-insensitive complex-value coherent receivers outperform intensity-only coherent receivers by approximately 3 dB, where part of the noise is squeezed from the amplitude dimension to the phase dimension during equalization. Fourth, an MZM transmitter with phase-sensitive complex-value coherent receivers has more than 6.3 dB higher sensitivity than EML-based phase-insensitive coherent receivers. The improvement is benefited by the removal of the DC component in the signal, and the increase in Euclidean distance by utilizing phase diversity. Finally, for the Alamouti-coding scheme, both polarization signals are included in the received optical power, while only one polarization of the signal can beat with the LO in the optical hybrid. Therefore, the 3 dB sensitivity penalty is compared with the MZM + 2 × 4 DP intradyne receiver.

To achieve 29 dB power budget, the 2 × 2 BPD-based heterodyne receiver needs 5 dBm launch power, while DD and the other intensity-only coherent receivers need larger than 6.5 dBm optical power. Therefore, transmitter-side optical amplification is suggested for DD and intensity-only coherent receivers. Compared with the 3 × 3 coupler and 2 × 4 hybrid-based receiver, the 2 × 2 coupler and BPD-based heterodyne detection is a better choice with a simpler structure, as long as the PD bandwidth is large enough. Moreover, both phase-insensitive and phase-sensitive complex-value coherent receivers satisfy the power budget requirement.

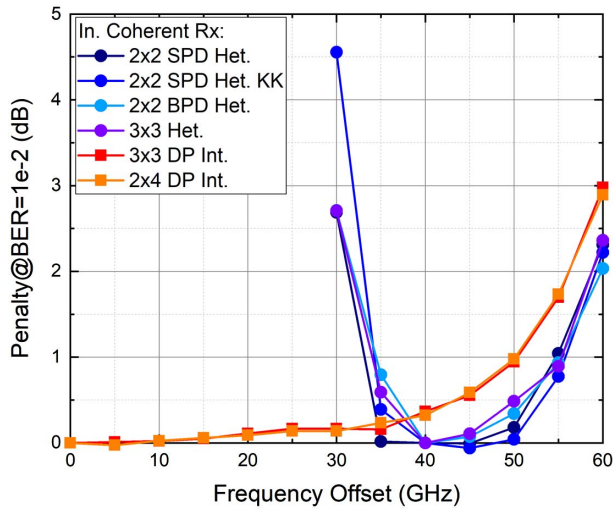


**Fig. 6.** Simulated sensitivity penalty versus frequency offset for different intensity-only coherent receivers at BTB, respectively.

**B. Frequency Offset**

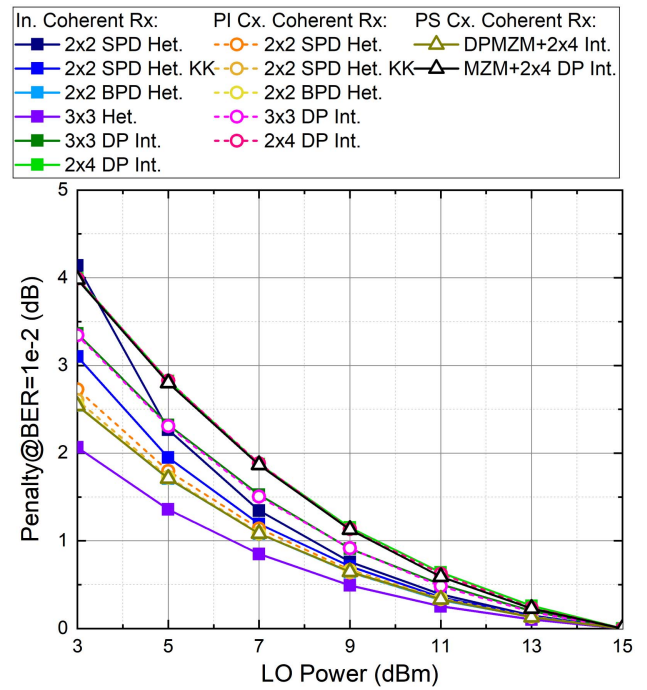
Unlike the colorless reception of the DD receiver, coherent receivers are inherently a kind of colored receiver. Based on this, the future wavelength plan and the requirement of laser drift would be closely related to the tolerance of frequency offset between the transmitter-side laser and LO.

Figure 6 shows the simulated sensitivity penalty versus frequency offset for different coherent detection receivers at BTB. Here we take intensity-only coherent receivers for examples. For a 0.5 dB penalty at a BER threshold of  $1 \times 10^{-2}$ , the frequency intervals of intradyne and heterodyne detection schemes are  $[-40 \text{ GHz}, 40 \text{ GHz}]$  and  $[30 \text{ GHz}, 50 \text{ GHz}]$ , respectively. In other words, the frequency offset tolerance is 80 GHz and 20 GHz for intradyne and heterodyne detection schemes, respectively. The reason is that, for heterodyne detection, smaller frequency offset would result in spectral overlap, while larger frequency offset is limited by the PD bandwidth-induced ISI. Therefore, temperature control is required if the coherent receiver is used.

**C. LO Power**

The sensitivities in Fig. 4 are given by setting the LO power as 15 dBm. However, for practical implementation, lower LO power is preferred to reduce the receiver-side power consumption. Figure 7 depicts the simulated sensitivity penalty versus LO power for different coherent detection receivers with intensity-only/complex-value equalization at BTB, respectively. At the BER threshold of  $1 \times 10^{-2}$ , the penalty at low LO power from smallest to largest is sorted as in Table 3.

The simulation results can be explained as follows: (1) Most of the PD noise is contributed by the thermal noise and shot noise. The shot noise of the PD is proportional to the input optical power, while the thermal noise is determined by the temperature. Therefore, sensitivity would gradually saturate to the shot noise limit as the LO power increases. (2) A coherent receiver with a larger number of coupler outputs



**Fig. 7.** Simulated sensitivity penalty versus LO power for intensity-only, phase-insensitive, and phase-sensitive coherent detection schemes at BTB, respectively.

**Table 3. Penalty at BER =  $1 \times 10^{-2}$  with 3 dBm LO Power**

Category	Scheme	Penalty (dB)
Phase-insensitive CRx	3 × 3 Het.	2.1
Intensity-only CRx	2 × 2 BPD Het.	2.5
Phase-insensitive CRx	2 × 2 SPD Het.	
	2 × 2 SPD Het. KK	
	3 × 3 Het.	
Phase-sensitive CRx	DPMZM + 2 × 4 Int.	
Intensity-only CRx	2 × 2 SPD Het.	3.1
Intensity-only CRx	3 × 3 DP Int.	3.4
Phase-insensitive CRx	3 × 3 DP Int.	
Intensity-only CRx	2 × 4 DP Int.	4.0
Phase-insensitive CRx	2 × 4 DP Int.	
Phase-sensitive CRx	MZM + 2 × 4 DP Int.	
Intensity-only CRx	2 × 2 SPD Het. KK	4.1

has lower input power for each PD, and thus worse performance is caused at low LO power due to the thermal noise. As a validation, 3 × 3 Het. Rx with 3 outputs shows the smallest penalty, while 2 × 4 DP int. Rx with 8 outputs has the largest penalty. (3) 2 × 2 SPD Het. Rx has a 4.1 dB penalty at 3dBm LO power. This is because the SSBI impairment becomes more severe as the LO-to-signal power ratio gets smaller. The 2 × 2 SPD Het. KK Rx also exhibits a slightly larger sensitivity penalty than the 2 × 2 BPD Het. Rx. The reason is that the SSBI cannot be perfectly compensated when the LO power is smaller than 5 dBm, in which case the minimum phase condition is no longer satisfied.

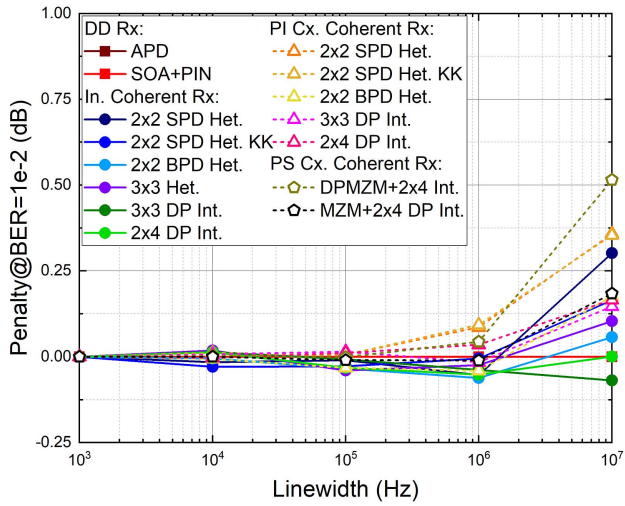


**Fig. 8.** Simulated sensitivity penalty versus frequency offset for different coherent receivers at BTB.

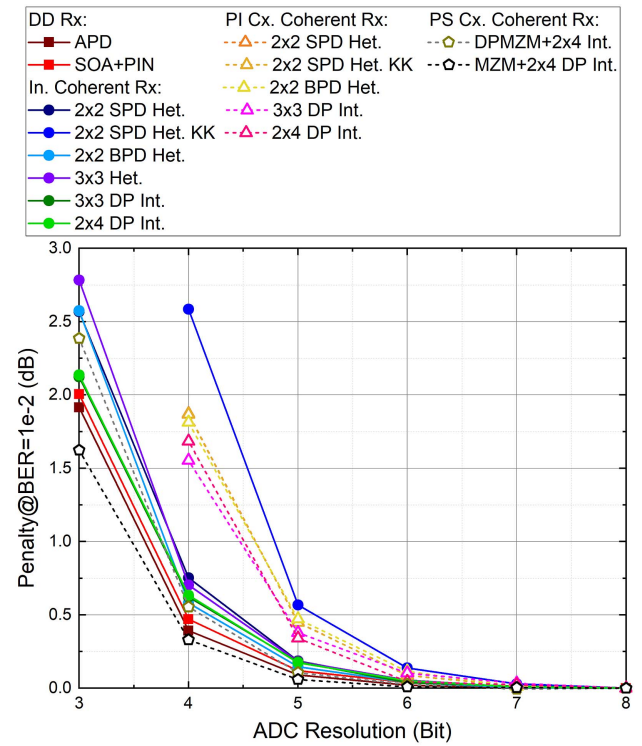
#### D. Laser Linewidth

Figure 8 shows the simulated sensitivity penalty versus transmitter-side laser linewidth for DD and coherent detection schemes at BTB, respectively. A negligible penalty can be observed for DD and intensity-only simplified coherent detection schemes. For phase-sensitive complex-value coherent receivers, we insert a pilot symbol in a 32-symbol block for phase noise estimation, and the powerful Viterbi–Viterbi phase estimation (VVPE) [33] and blind phase search (BPS) [34] algorithms are not applied. The simulation results indicate that a 10 MHz linewidth would induce only a 0.5 dB sensitivity penalty, which confirms the feasibility of using large linewidth lasers for low-cost coherent PON.

#### E. ADC Resolution

For DSP-based DD and coherent detection schemes, DAC/ADC resolution would be of importance for practical applications. Since no pulse shaping is used at the transmitter, a 2-bit DAC is enough to generate a PAM-4 signal. So we focus on the influence of ADC resolution. Figure 9 shows the simulated sensitivity penalty versus ADC resolution for DD and coherent detection schemes at BTB, respectively.

Several properties of the DD and coherent detection schemes can be obtained: (1) At the BER threshold of  $1 \times 10^{-2}$ ,  $2 \times 2$  SPD Het. KK Rx has the largest sensitivity penalty, which is 2.6 dB with a 4-bit ADC. The penalty comes from the nonlinear operations such as logarithm, Hilbert transform, and square. (2) Phase-insensitive complex-value coherent receivers also have a more than 1.5 dB penalty with a 4-bit ADC. This is because the DC optical component would rotate with phase noise, occupying part of the ADC resolution. (3) Compared with phase-sensitive complex-value coherent receivers, intensity-only coherent receivers have 1 bit lower requirement for an ADC. The reason is that the square operation in the analog process circuit confirms positive waveforms to the ADC, and the dynamic range of the signal amplitude is thus reduced. (4) Heterodyne detection is more sensitive to



**Fig. 9.** Simulated sensitivity penalty of ADC resolution for DD, intensity-only, phase-insensitive, and phase-sensitive coherent receivers, respectively.

ADC resolution than intradyne detection, where the in-phase and quadrature components are mixed in the IF with higher PAPR for heterodyne detection. (5) MZM +  $2 \times 4$  DP Int. Rx has the lowest requirement on the ADC, since the optical carrier is suppressed by a biasing MZM at the null point.

#### F. Fiber Dispersion

So far, we have studied several parameters in a BTB scenario. According to the previous standard, PON should support transmission distance up to 20 km. If a wavelength range of  $1342 \pm 2$  nm is chosen with G.652 fiber, the maximum accumulated dispersion would be approximately 75 ps/nm for the worst case. Therefore, it is necessary to investigate the dispersion tolerance of all the DD and coherent receivers at the O-band. Note that the chirp factor of the EML is set as 1, and the MZM is chirp-free thanks to its push-pull mode. First of all, as shown in Fig. 10(a), only a feed forward equalizer (FFE) is applied for dispersion compensation, where an ADC is ideal with infinite quantization resolution. Table 4 sorts the penalty of these schemes with 60 ps/nm fiber dispersion from smallest to largest.

One can find the following: (1) APD, SOA + PIN,  $3 \times 3$  DP Int. (In. CRx), and  $2 \times 4$  DP Int. (In. CRx) are severely affected by large positive dispersion. The penalty comes from the dispersion induced power fading effect, since the phase information is lost during PD detection or after the analog process circuit. (2) In contrast, the penalty can be reduced by using intensity-only heterodyne coherent receivers. During PD detection, power fading is avoided by heterodyne detection.

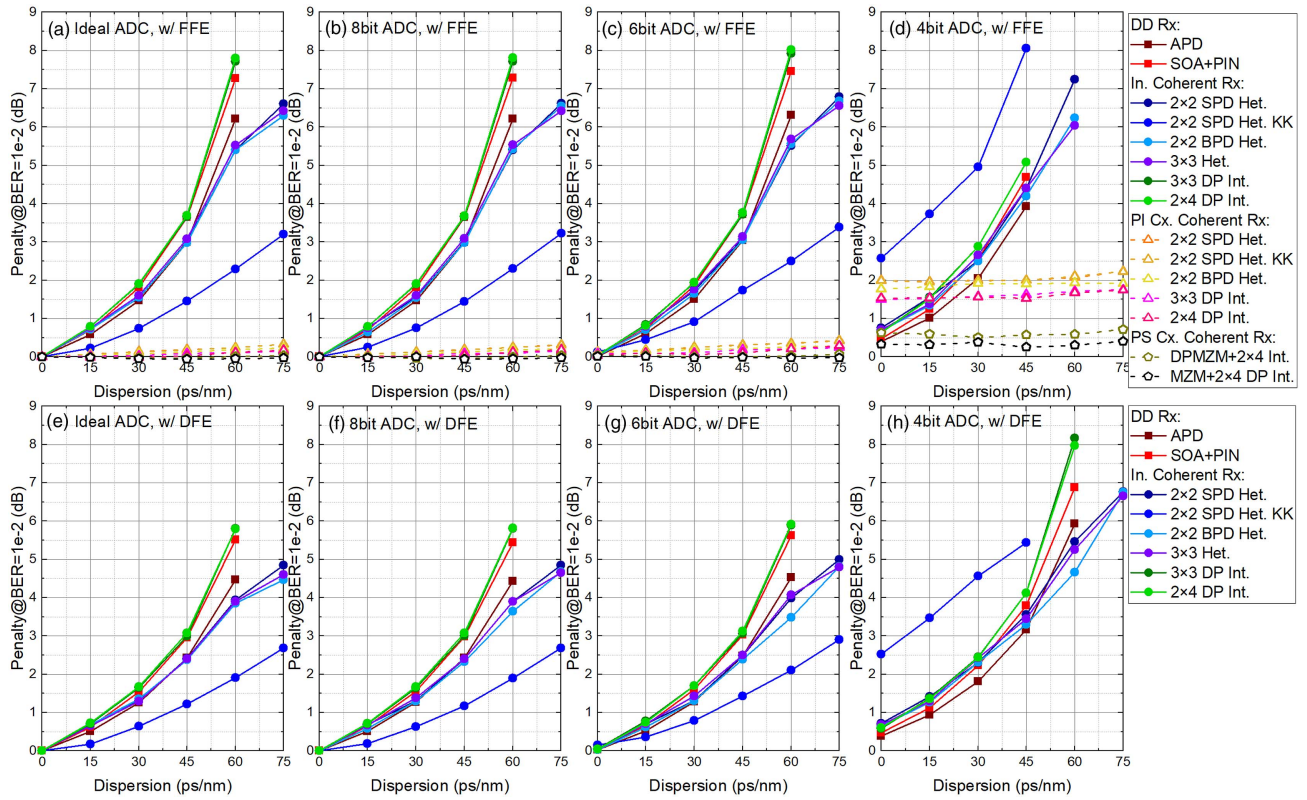


**Fig. 10.** Simulated fiber dispersion penalty with FFE: (a) ideal ADC, (b) 8 bit ADC, (c) 6 bit ADC, and (d) 4 bit ADC; and with FFE + DFE: (e) ideal ADC, (f) 8 bit ADC, (g) 6 bit ADC, and (h) 4 bit ADC, respectively. w/, with.

Afterwards, part of the upper sideband of the signal is filtered by the PD bandwidth, and the following analog process circuit squares vestigial sideband (VSB) signal, leading to weak power fading. (3)  $2 \times 2$  SPD Het. KK Rx can reconstruct the complex optical field, achieving better dispersion tolerance even if intensity-only reception is applied later. (4) For both phase-insensitive and phase-sensitive coherent receivers, dispersion-induced ISI becomes a linear impairment and thus can be efficiently mitigated by complex equalization.

Second, the influence of ADC resolution on the dispersion compensation performance with FFE is also presented in Figs. 10(b)–10(d). It can be confirmed that 6 bit ADC resolution is enough for practical implementation, since the additional penalty is negligible compared with an ideal ADC. When the ADC resolution decreases to 4 bit,  $2 \times 2$  SPD Het. KK intensity-only and phase-insensitive complex-value coherent receivers suffer from large additional penalties of 5 dB and 1.6 dB at 60 ps/nm fiber dispersion, respectively. The former is degraded by the imprecise nonlinear operations, while the latter results from the DC component of the signal.

Moreover, the decision feedback equalizer (DFE) is also a powerful algorithm to compensate for ISI. Figures 10(e)–10(h) provide the fiber dispersion penalty by using FFE + DFE under different ADC resolutions, respectively. Here neither phase-insensitive nor phase-sensitive complex-value coherent receivers are considered because FFE is enough for these schemes. At 60 ps/nm fiber dispersion with an ideal ADC, a larger than 1.5 dB penalty reduction can be achieved with

**Table 4.** Penalty at BER =  $1 \times 10^{-2}$  with 60 ps/nm Fiber Dispersion and an Ideal ADC

Category	Scheme	Penalty (dB)
Phase-sensitive CRx	MZM + $2 \times 4$ DP Int.	<0.1 dB
	DPMZM + $2 \times 4$ Int.	
Phase-insensitive CRx	$2 \times 2$ SPD Het.	<0.3 dB
	$2 \times 2$ SPD Het. KK	
	$2 \times 2$ BPD Het.	
	$3 \times 3$ Het.	
	$3 \times 3$ DP Int.	
Intensity-only CRx	$2 \times 2$ SPD Het. KK	2.3
	$2 \times 2$ SPD Het.	5.4
DD Rx	$2 \times 2$ BPD Het.	6.2
	$3 \times 3$ Het.	
	APD	
	SOA + PIN	
Intensity-only CRx	$3 \times 3$ DP Int.	7.7
	$2 \times 4$ DP Int.	

FFE + DFE for DD and intensity-only coherent receivers (except for  $2 \times 2$  SPD Het. KK Rx) compared with FFE only. Benefiting from the structure of the feedback loop, the dispersion-induced power fading in the frequency domain can be partially compensated. However, the penalty of DD and intensity-only coherent receivers still cannot be reduced to below 1 dB at an accumulated dispersion value of 75 ps/nm.

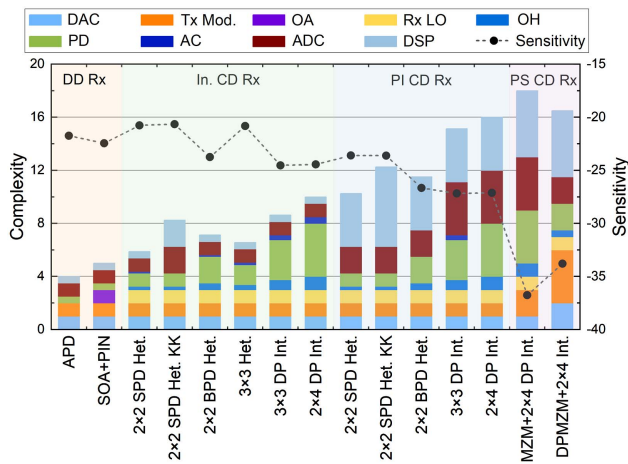


**Fig. 11.** Hardware complexity and sensitivity of DD: intensity-only, phase-insensitive, and phase-sensitive coherent receivers, respectively. Mod., modulator; OA, optical amplifier; OH, optical hybrid; AC, analog process circuit; In., intensity-only; PI, phase-insensitive; PS, phase-sensitive.

As a consequence, the zero-dispersion wavelength range is suggested for DD and intensity-only coherent receivers.

### G. Hardware Complexity

Figure 11 plots the hardware complexity and sensitivity of DD and coherent detection schemes, respectively. Note that it is difficult to fairly compare the complexity of different system parts, and the weight coefficient of each part [DAC, transmitter-side modulator (Mod.), optical amplifier (OA), LO, optical hybrid (OH), PD, analog process circuit (AC), ADC, and DSP] is set as 1:1:1:1:0.5:0.5:0.125:1:0.5 for simplicity.

The specific complexity comes from the following considerations: (1) For the DPMZM + 2 × 4 Int. scheme, the transmitter-side hardware complexity including the DAC and modulator is doubled due to the implementation of polarization-time coding. (2) An optical amplifier is only needed for the SOA + PIN DD scheme, and a LO is required for all the coherent receivers. (3) The complexity of optical hybrids and the analog process circuit are quantitated by the number of outputs and the number of multiplication circuits, respectively. (4) For DD and intensity-only coherent receivers (except 2 × 2 SPD Het. KK Rx), only a one-channel ADC is needed, while the other coherent detection schemes need multiple ADCs proportional to the number of optical hybrid outputs. (5) The complexity of DSP is determined by the number of multiplication operations. For the KK algorithm, 4 SPSs are used for both polarization waveforms instead of 2, so as to protect the high-order terms induced by nonlinear operations. For equalization in both phase-insensitive and phase-sensitive coherent receivers, the multiplication of complex numbers is 4 times more complicated than real numbers. Moreover, pilot symbol-based phase recovery contributes one complex multiplication per symbol for phase-sensitive coherent receivers.

Generally, better receiver sensitivity can be gained by more complicated transceiver structures. Compared with the 2 × 2 SPD Het. scheme, KK coherent receivers consume quite a lot of computational complexity in DSP, which does not bring enough benefits. For phase-insensitive coherent receivers, the complexity mainly arises from the multi-channel ADCs and complex number operations in DSP. For phase-sensitive coherent receivers, additional complexity comes from the MZM or DPMZM. Although heterodyne detection requires a higher bandwidth receiver and has worse tolerance of laser frequency offset, the receiver structure is simpler than the intradyne receiver. Moreover, if both upstream and downstream cases are considered, heterodyne detection is more efficient since each laser at the ONU or OLT can act as a source laser and LO simultaneously [14,16]. From this perspective, heterodyne detection with low-complexity equalizers would be a promising choice compared with intradyne detection.

### 4. CONCLUSION

In this paper, we carry out a comparative study on various cost-effective coherent detection and DD schemes for future 100 Gb/s/λ PON through numerical simulation. We investigate three levels of coherent receivers based on the cost: intensity-only coherent receivers and phase-insensitive and phase-sensitive complex-value coherent receivers. The receiver power sensitivity at BTB, the influence of frequency offset, LO power, laser linewidth, ADC resolution, fiber dispersion, and hardware complexity are evaluated. We conclude the following: (1) Transmitter-side optical amplification is suggested for DD and intensity-only coherent receivers to meet the 29 dB power budget requirement, and these schemes show a large dispersion penalty. (2) Compared with a 3 × 3 coupler and a 2 × 4 hybrid-based receiver, 2 × 2 coupler and BPD-based heterodyne detection exhibit similar performance with simpler structure. (3) Both phase-insensitive and phase-sensitive complex-value coherent receivers have superior power budget and dispersion tolerance; the main limitation for them would be the cost. We believe the performance comparison in this paper provides a valuable reference for the selection of next generation PON solutions.

**Funding.** National Key Research and Development Program of China (2018YFB1800904); National Natural Science Foundation of China (61431009).

### REFERENCES

1. "Physical Layer Specifications and Management Parameters for 25 Gb/s and 50 Gb/s Passive Optical Networks," IEEE 802.3ca Task Force, <http://www.ieee802.org/3/ca/index.shtml>.
2. V. Houtsma, D. van Veen, and E. Harstead, "Recent progress on standardization of next-generation 25, 50, and 100G EPON," *J. Lightwave Technol.* **35**, 1228–1234 (2017).
3. J. S. Wey, "The outlook for PON standardization: a tutorial," *J. Lightwave Technol.* **38**, 31–42 (2020).
4. "Optical systems for fibre access networks," ITU-T Q2/SG15, <https://www.itu.int/en/ITU-T/studygroups/2017-2020/15/Pages/q2.aspx>.
5. J. Zhang, J. Yu, H. Chien, J. S. Wey, M. Kong, X. Xin, and Y. Zhang, "Demonstration of 100-Gb/s/λ PAM-4 TDM-PON supporting 29-dB

- power budget with 50-km reach using 10G-class O-band DML transmitters,” in *Optical Fiber Communication Conference* (2019), paper Th4C.3.
6. L. Yi, T. Liao, L. Huang, L. Xue, P. Li, and W. Hu, “Machine learning for 100 Gb/s/λ passive optical network,” *J. Lightwave Technol.* **37**, 1621–1630 (2019).
  7. J. Zhang, J. S. Wey, J. Shi, and J. Yu, “Single-wavelength 100-Gb/s PAM-4 TDM-PON achieving over 32-dB power budget using simplified and phase insensitive coherent detection,” in *European Conference on Optical Communication* (2018), paper Tu1B.1.
  8. J. Zhang, J. Yu, X. Li, K. Wang, W. Zhou, J. Xiao, L. Zhao, X. Pan, B. Liu, and X. Xin, “200 Gbit/s/λ PDM-PAM-4 PON system based on intensity modulation and coherent detection,” *J. Opt. Commun. Network.* **12**, A1–A8 (2020).
  9. D. Che, Q. Hu, and W. Shieh, “Linearization of direct detection optical channels using self-coherent subsystems,” *J. Lightwave Technol.* **34**, 516–524 (2016).
  10. V. Houtsma and D. van Veen, “Bi-directional 25G/50G TDM-PON with extended power budget using 25G APD and coherent detection,” *J. Lightwave Technol.* **36**, 122–127 (2018).
  11. M. S. Erkiñç, D. Lavery, K. Shi, B. C. Thomsen, P. Bayvel, R. I. Killey, and S. J. Savory, “Polarization-insensitive single-balanced photodiode coherent receiver for long-reach WDM-PONs,” *J. Lightwave Technol.* **34**, 2034–2041 (2016).
  12. M. S. Erkiñç, R. Emmerich, K. Habel, V. Jungnickel, C. Schmidt-Langhorst, C. Schubert, and R. Freund, “PON transceiver technologies for  $\geq 50$  Gbits/s per  $\lambda$ : Alamouti coding and heterodyne detection [Invited],” *J. Opt. Commun. Netw.* **12**, A162–A170 (2020).
  13. H. Li, M. Luo, X. Li, X. Zhang, and S. Yu, “Demonstration of polarization-insensitive coherent 56 Gb/s/λ PAM-4 PON using real-valued Alamouti coding combined with digital pilot,” in *European Conference on Optical Communication* (2019), paper M.1.F.4.
  14. D. Lavery, T. Gerard, S. Erkiñç, Z. Liu, L. Galdino, P. Bayvel, and R. I. Killey, “Opportunities for optical access network transceivers beyond OOK [Invited],” *J. Opt. Commun. Netw.* **11**, A186–A195 (2019).
  15. M. S. Erkiñç, D. Lavery, K. Shi, B. C. Thomsen, R. I. Killey, S. J. Savory, and P. Bayvel, “Comparison of low complexity coherent receivers for UDWDM-PONs ( $\lambda$ -to-the-user),” *J. Lightwave Technol.* **36**, 3453–3464 (2018).
  16. A. Shahpari, R. M. Ferreira, R. S. Luis, Z. Vujcic, F. P. Guiomar, J. D. Reis, and A. L. Teixeira, “Coherent access: a review,” *J. Lightwave Technol.* **35**, 1050–1058 (2017).
  17. Y. Zhu, B. Yang, Y. Zhong, Z. Liu, Y. Guo, J. S. Wey, X. Huang, and Z. Ma, “Performance comparison of coherent and direct detection schemes for 50G PON,” in *Optical Fiber Communication Conference* (2020), paper W1E.3.
  18. B. Glance, “Polarization independent coherent optical receiver,” *J. Lightwave Technol.* **5**, 274–276 (1987).
  19. A. Mecozzi, C. Antonelli, and M. Shtaif, “Kramers–Kronig coherent receiver,” *Optica* **3**, 1220–1227 (2016).
  20. Z. Li, M. Erkiñç, K. Shi, E. Sillekens, L. Galdino, B. Thomsen, P. Bayvel, and R. Killey, “SSBI mitigation and the Kramers–Kronig scheme in single-sideband direct-detection transmission with receiver-based electronic dispersion compensation,” *J. Lightwave Technol.* **35**, 1887–1893 (2017).
  21. S. T. Le, K. Schuh, M. Chagnon, F. Buchali, R. Dischler, V. Aref, H. Buelow, and K. M. Engenhardt, “1.72 Tb/s virtual-carrier assisted direct-detection transmission over 200 km,” *J. Lightwave Technol.* **36**, 1347–1353 (2018).
  22. X. Chen, C. Antonelli, S. Chandrasekhar, G. Raybon, A. Mecozzi, M. Shtaif, and P. Winzer, “Kramers–Kronig receivers for 100-km datacenter interconnects,” *J. Lightwave Technol.* **36**, 79–89 (2018).
  23. Y. Zhu, K. Zou, X. Ruan, and F. Zhang, “Single carrier 400G transmission with single-ended heterodyne detection,” *IEEE Photon. Technol. Lett.* **29**, 1788–1791 (2017).
  24. E. Ciaramella, “Polarization-independent receivers for low-cost coherent OOK systems,” *IEEE Photon. Technol. Lett.* **26**, 548–551 (2014).
  25. Y. H. Ja, “Analysis of four-port optical fiber ring and loop resonators using a  $3 \times 3$  fiber coupler and degenerate two-wave mixing,” *IEEE J. Quantum Electron.* **28**, 2749–2757 (1992).
  26. E. Ciaramella, “Assessment of a polarization-independent DSP-free coherent receiver for intensity-modulated signals,” *J. Lightwave Technol.* **38**, 676–683 (2020).
  27. C. Xie, P. J. Winzer, G. Raybon, A. H. Gnauck, B. Zhu, T. Gersler, and B. Edvold, “Colorless coherent receiver using  $3 \times 3$  coupler hybrids and single-ended detection,” *Opt. Express* **20**, 1164–1171 (2012).
  28. I. Fatadin, D. Ives, and S. J. Savory, “Blind equalization and carrier phase recovery in a 16-QAM optical coherent system,” *J. Lightwave Technol.* **27**, 3042–3049 (2009).
  29. S. J. Savory, “Digital coherent optical receivers: algorithms and subsystems,” *IEEE J. Sel. Top. Quantum Electron.* **16**, 1164–1179 (2010).
  30. J. Zhang, J. S. Wey, J. Shi, J. Yu, Z. Tu, B. Yang, W. Yang, Y. Guo, X. Huang, and Z. Ma, “Experimental demonstration of unequally spaced PAM-4 signal to improve receiver sensitivity for 50-Gbps PON with power-dependent noise distribution,” in *Optical Fiber Communication Conference* (2018), paper M2B.3.
  31. M. Nazarathy, B. Livshitz, Y. Atzmon, M. Secondini, and E. Forestieri, “Optically amplified direct detection with pre- and post-filtering: a Volterra series approach,” *J. Lightwave Technol.* **26**, 3677–3693 (2008).
  32. V. Houtsma, E. Chou, and D. van Veen, “92 and 50 Gbps TDM-PON using neural network enabled receiver equalization specialized for PON,” in *Optical Fiber Communication Conference* (2019), paper M2B.6.
  33. K. Kikuchi, “Phase-diversity homodyne detection of multilevel optical modulation with digital carrier phase estimation,” *IEEE J. Sel. Top. Quantum Electron.* **12**, 563–570 (2006).
  34. T. Pfau, S. Hoffmann, and R. Noé, “Hardware-efficient coherent digital receiver concept with feedforward carrier recovery for M-QAM constellations,” *J. Lightwave Technol.* **27**, 989–999 (2009).